Murat Serhatlioglu[1]
Mohammad Asghari[1]
Mustafa Tahsin Guler[2]
Caglar Elbuken[1]

[1]UNAM–National Nanotechnology Research Center and Institute of Materials Science and Nanotechnology, Bilkent University, Ankara, Turkey
[2]Department of Physics, Kirikkale University, Kirikkale, Turkey

Received August 28, 2018
Revised December 13, 2018
Accepted December 19, 2018

Research Article

Impedance-based viscoelastic flow cytometry

Elastic nature of the viscoelastic fluids induces lateral migration of particles into a single streamline and can be used by microfluidic based flow cytometry devices. In this study, we investigated focusing efficiency of polyethylene oxide based viscoelastic solutions at varying ionic concentration to demonstrate their use in impedimetric particle characterization systems. Rheological properties of the viscoelastic fluid and particle focusing performance are not affected by ionic concentration. We investigated the viscoelastic focusing dynamics using polystyrene (PS) beads and human red blood cells (RBCs) suspended in the viscoelastic fluid. Elasto-inertial focusing of PS beads was achieved with the combination of inertial and viscoelastic effects. RBCs were aligned along the channel centerline in parachute shape which yielded consistent impedimetric signals. We compared our impedance-based microfluidic flow cytometry results for RBCs and PS beads by analyzing particle transit time and peak amplitude at varying viscoelastic focusing conditions obtained at different flow rates. We showed that single orientation, single train focusing of nonspherical RBCs can be achieved with polyethylene oxide based viscoelastic solution that has been shown to be a good candidate as a carrier fluid for impedance cytometry.

Keywords:
Impedance cytometry / Microfluidics / Rheology / Single cell characterization / Viscoelastic focusing
DOI 10.1002/elps.201800365

Additional supporting information may be found online in the Supporting Information section at the end of the article.

1 Introduction

Precise particle focusing is critical for a variety of biological and chemical microfluidic applications. In the field of flow cytometry, suspended particles aligned along the centerline of a conduit is necessary to achieve high signal repeatability and low coefficient of variation (CV). To this end, externally applied electric [1, 2], acoustic [3, 4], magnetic [5], optical [6] forces as well as flow-induced inertial [7–9], elastic [10–13], and Dean-drag forces [14, 15] were successfully implemented in microfluidic systems.

Flow-induced lift forces provide passive manipulation of particles with less effort and are advantageous over externally applied forces. Inertial lift and drag forces were utilized in inertial microfluidics for Newtonian fluids using straight channels and/or curvatures [16, 17]. These systems require high flow rates and complex microchannel geometries to obtain a single train of particles, which is considered as a bottleneck for cytometry implementations due to faster signal processing requirements and fabrication difficulties [18].

As a recently trending technique, viscoelastic focusing is a cut above the rest of the techniques. Some recent review articles cover the viscoelastic focusing theory, device implementations, application fields, and future aspects [19, 20]. Viscoelastic fluids are prepared by dissolving biological or synthetic polymeric substances in Newtonian solvents. Flow-induced elastic lift force originates from the normal stress gradients. This lift force provides precise position control and fixed orientation across the channel cross section for suspended particles. Unlike inertial microfluidics, viscoelastic fluids can manipulate particles even at low flow rates (on the order of μl/h). When elastic lift force is accompanied with inertial lift force, referred as elasto-inertial or inertio-elastic focusing [21], it supports focusing at high flow rates up to ml/s [9, 18, 22–25].

Viscoelastic and elasto-inertial focusing have been investigated for different synthetic and biological particles such as polystyrene beads (PS), blood cells [21, 26–30], MCF-7 cells [31], sperm cells [32], Jurkat cells [33], and

Correspondence: Dr. Caglar Elbuken, Bilkent University, UNAM, Eskisehir yolu 8. km, 06800, Cankaya, Ankara, Turkey
Fax: +90 (312) 2664365
E-mail: elbuken@unam.bilkent.edu.tr

Abbreviations: HA, Hyaluronic acid; **PEO**, polyethylene oxide; **PS**, polystyrene; **RBCs**, red blood cells

Color online: See the article online to view Figs. 1–5 in color.

bacteria [18, 31, 34, 35]. Viscoelastic fluids have been prepared by dissolving polymeric (polyethylene oxide [18, 27, 29, 34], polyacrylamide [36], and polyvinylpyrrolidone [12, 26, 28]) or biological (hyaluronic acid [16, 21, 33] and λ-DNA [37]) substances in Newtonian fluids. Viscoelastic solutions are mostly biocompatible but may require further attention to ensure cell viability. Typically, 1X PBS is added to the viscoelastic solution to increase the cell viability. However, addition of a salt buffer solution may cause undesired changes in the rheological properties of viscoelastic solutions. For example, Giudice et al. reported that addition of PBS to hyaluronic acid (HA) solution results in polymer shrinkage and impedes the shear thinning properties of the viscoelastic solution [33].

Microfluidic impedance based cytometers measure cellular biophysical properties with electrical impedance measurements [38]. Prior to the measurement, particles are dispensed in ionic buffers (e.g., PBS) or electrolyte solutions. Then, impedance signals are acquired at electrical detection region from individual cells aligned in a single stream. Thus, the ionic concentration of the solution is critical and has to be adjusted to generate a contrast between the impedance of the particles and the suspending medium to ensure selectivity and high signal to noise ratio [39, 40]. Viscoelastic focusing has been straightforwardly applied in optical cytometry applications [18, 41, 42]. However, implementation of viscoelastic solutions in impedance-based systems requires the analysis of the ionic buffer concentration and its effect on viscoelastic focusing due to potential coupling of rheological and electrical properties of the carrier solution.

In this study, we present an impedance-based microfluidic flow cytometry device using polyethylene oxide (PEO) viscoelastic solutions. First, the dynamic viscosity of different molecular weight (M_w) and concentration of PEO polymer solutions were characterized to obtain constant viscosity over a wide range of shear rates to support stable particle focusing. Then, the effect of varying ionic concentrations of PBS (1X, 3X, 10X) on the rheological properties of PEO solutions was assessed. Later, particle focusing efficiency was observed in different ionic concentration viscoelastic solutions inside square cross section microchannels. Focusing of 6 μm diameter PS beads was observed in a range of Reynolds (Re) and Weissenberg (Wi) numbers ($0.04<Re<32$, $3.9<Wi<2968$). Next, human RBCs were used in 1X-PBS/PEO solution to observe the focusing and orientation of cells in the $0.002<Re<0.44$ range. Finally, impedance flow cytometry measurements were demonstrated for PS beads and RBCs suspended in 1X-PBS/PEO viscoelastic solutions and the device performance was analyzed.

2 Materials and methods

2.1 Solution preparation

Three sets of viscoelastic solutions were prepared for the characterization of rheological properties (Anton Paar, MCR 301): i) Four different molecular weights of PEO polymer (M_w = 0.1, 0.6, 0.9, and 5 MDa, Sigma-Aldrich) were dissolved in DI water to a concentration of 1000 ppm. ii) PEO_{5MDa} was dissolved in DI water at five different concentrations (500, 1000, 2500, 5000, and 10000 ppm). iii) PEO_{5MDa} was dissolved in three PBS solutions (1X, 3X, and 10X) to a concentration of 1000 ppm.

2.2 Particle suspensions

Spherical polystyrene particles of 6.0 μm diameter (Polysciences, Inc.) were suspended in viscoelastic solutions of 1X-PBS/PEO, 3X-PBS/PEO, and 10X-PBS/PEO at a concentration of 10^3 particles/ml. During the experiments, particles at the inlet were continuously mixed with a magnetic stirrer to keep the particle concentration uniform. 50 μl whole blood was finger pricked from a volunteer and immediately mixed with 10 μl EDTA (1.5 mg/ml) in an anticoagulant tube. Later, blood samples were added to 1 mL 1X-PBS solution and centrifuged at 5000 rpm for 3 min. Finally 5 μl of precipitated RBCs was dispensed in 5 mL 1X-PBS/PEO viscoelastic solution to a dilution of 1:1000 ratio.

2.3 Device fabrication

The details of fabrication steps are explained in supplementary file. Briefly, the microfluidic device consists of three parts: 6 cm long 30×30 μm^2 square cross-sectional PDMS microchannel, three Cr/Au (10 μm wide, and 10 μm gap) coplanar microelectrodes on 25×75 mm^2 glass slide, and a laser-cut PMMA clamp. We aligned the PDMS channel layer to the electrode-patterned glass substrate and brought them in contact without any plasma treatment. Then, we sandwiched the PDMS and glass layers between two PMMA plates using screws for reusability of the microfabricated electrodes [39].

3 Results and discussion

3.1 Measurement setup and working principle

The schematic impedance based cytometry device is shown in Fig. 1. It consists of a single inlet/outlet PDMS channel and three coplanar electrodes. Particles suspended in viscoelastic solutions are sent through the inlet and collected at the outlet. At specific flow conditions, due to the elastic lift or combination of both elastic and inertial lift forces, particles migrate to the center of the channel and a single train of particles is reached upstream the impedance sensing region. Electrodes are used in differential configuration for electrical impedance measurements. Center electrode is stimulated with 1 V_{p-p} bias voltage at 2.5 MHz AC signal, which is generated using the internal signal generator of HF2LI Lock-in Amplifier (Zurich Instruments). Currents are collected from two side electrodes and converted to voltage using HF2TA transimpedance amplifier (Zurich Instruments). Voltage signal is fed back

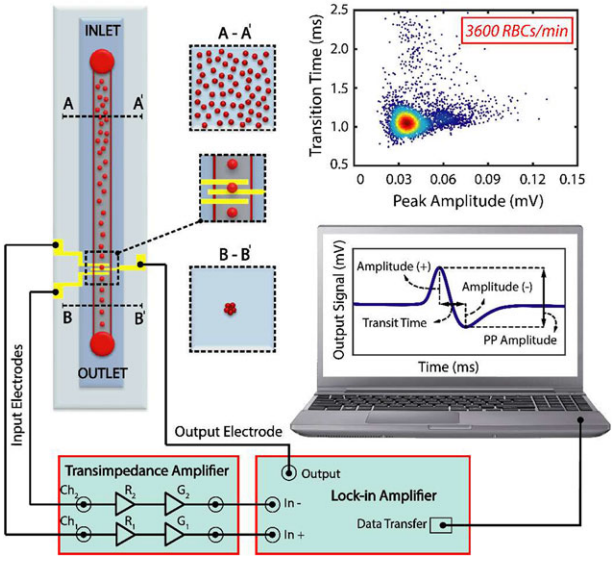

Figure 1. Illustration of the impedance-based viscoelastic flow cytometer. Particles suspended in viscoelastic solution are pumped through the microchannel and focused at the center of the channel as shown in the channel cross section profile, B-B′. Particles are detected by a lock-in amplifier using three coplanar electrodes in differential configuration. Each event is characterized by its transit time and peak amplitude.

to the lock-in amplifier and demodulated. Fourth order 1 kHz bandwidth, low-pass filter is selected for demodulation at 100 kSa/s. To inspect the performance of the device, PS beads and RBCs are pumped through the inlet of the channel at varying pressures from 50 to 200 mbar for PS beads and from 50 to 400 mbar for RBCs. Resulting signals are exported to a PC and post processed using Matlab to acquire peak amplitude (peak-to-peak voltage/2) and transition time of particles. Finally, CV values for each inlet pressure value are compared.

3.2 Solution characterization

The rheological properties of a viscoelastic fluid are important for the performance of viscoelastic focusing and equilibrium position of particles in fluidic channel [43]. We characterized the viscoelastic solutions for varying polymer length (M_w), polymer concentration and ionic salt concentration to understand the rheological changes. The results of these rheology measurements are given in Fig. 2. We used a cone and plate (CP) measurement fixture CP50-1 (50 mm diameter, 1° cone angle) to provide homogenous shear conditions.

Shear viscosity measurements of four different M_w, PEO solutions of same concentration (0.1% w/v) are given in Fig. 2A. High M_w viscoelastic solutions have higher elasticity since they exhibit longer relaxation time and higher viscosities. PEO_{5MDa} solution exhibits higher shear viscosity compared to low M_w solutions. Following characterizations were performed with PEO_{5MDa}.

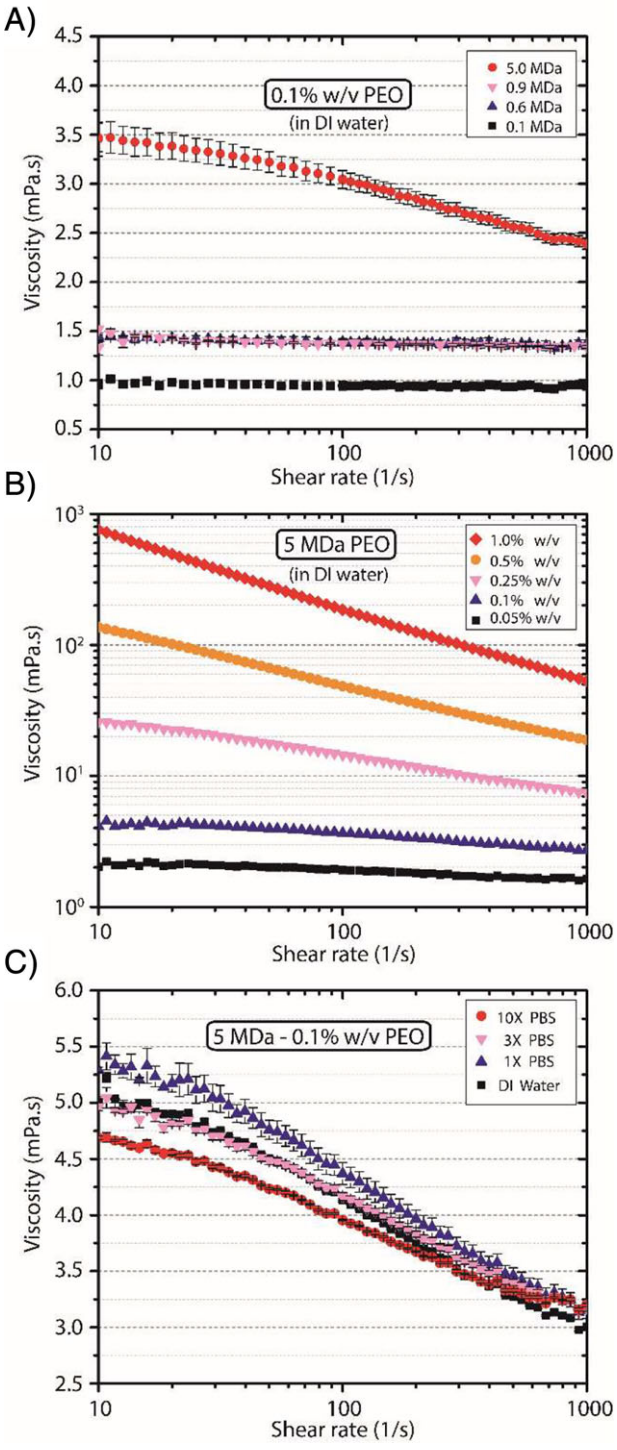

Figure 2. Shear rate dependence of viscosity of PEO solutions: (A) four different M_w PEO solutions at 0.1% w/v concentration, the error bars represent 2 S.D. of $n = 5$ measurements (B) five concentrations of PEO_{5MDa} solution (the error bars are smaller than the measurement markers) and (C) 0.1% w/v PEO_{5MDa} solution at three ionic concentrations and DI.

Figure 2.B shows shear viscosity measurements of PEO_{5MDa} for five different concentrations. It is important to keep the solution at constant shear viscosity range, since particles in shear thinning liquids show tendency to migrate away from the center to the walls of the channel [10, 33]. The low concentration solution, 0.05% of PEO_{5MDa}, shows almost shear constant viscosity that is desired for efficient particle focusing. On the other hand, the high concentration solutions (≥0.1% w/v) yield a shear thinning profile. Thus, 0.05% w/v PEO_{5MDa} is chosen for the flow focusing experiments.

Yu et al. performed a series of rheometer measurements to show the effect of NaCl added into a PEO solution and demonstrated that the rheological properties are insensitive to the addition of NaCl up to 2% w/w in 10% w/w concentration PEO_{2MDa} solution [44]. PBS includes various salts and its behavior in PEO based viscoelastic solutions needs to be characterized prior to impedance cytometry measurements. Viscoelastic solutions were prepared in three varying concentrations of PBS with constant polymeric concentration. As shown in Fig. 2C, we observed negligible change in viscosities for varying ionic buffer concentrations. These results reveal that the concentration of ionic buffer in PEO based viscoelastic solutions has negligible effect on viscosity, thus the rheological and the impedimetric properties of the solution can be adjusted independently.

3.3 Flow focusing of particles

Rheometer measurements in the previous section give an insight to the effect of PBS in viscoelastic PEO solution. It is still required to observe particle migration and focusing dynamics (elastic or elasto-inertial) for different PBS concentrations in microchannels.

500 ppm PEO_{5MDa} viscoelastic solutions were prepared in three different PBS concentrations (1X, 3X, and 10X). Then, 6 μm PS beads were pipetted (10^3 particles/ml) to the prepared solutions and were pumped through the microchannels using a syringe pump (KDS 100). Particle focusing at varying flow rates was observed and recorded at 5000 fps using an inverted optical microscope (Zeiss) equipped with high-speed camera (Phantom Miro e2) as given in Figs. 3A and B. Recorded videos were split to single frames and image stacked to form a single picture.

In Fig. 3A, at low flow rates (<20 μl/h), PS particles migrate both to the center and corners of the channel, which corresponds to low first normal stress difference regions [9], when inertial lift force is negligible (Re<0.1). When the flow rate is increased until 40 μl/h, corner-aligned particles migrate to the center of the channel due to the contribution of inertial lift forces. Particles closer to the walls are under the influence of wall-induced lift force and migrate to the center of the channel by increasing the flow rate. For flow rates between 40 (Re: 0.17) to 950 μl/h (Re: 4.0), the particles are aligned at the centerline thanks to the contribution of inertial lift force. Central particle trajectory starts to deteriorate at higher flow rates above 950 μl/h due to conquering of the inertial lift forces over elastic forces. We observed a disturbed particle train at the flow rates above 1900 (Re: 8.0) to 7600 μl/h (Re: ~32.0). At high flow rates, due to image blurriness, we presented snapshot images (instead of image-stack). Recently, Kim et al. successfully achieved elasto-inertial focusing at high flow rates (1300 μl/h) using λ-DNA solution [37]. Lim et al. showed elasto-inertial focusing at extremely high flow rates (50 mL/min) using HA based solution [21]. However, these biological solutions use polymers that carry ionic side chains. In such a case addition of ionic buffer changes the rheological properties of solutions that leads to deterioration of particle focusing efficiency [33].

In Fig. 3B, we observed almost identical focusing profiles for two other PBS-based (3X and 10X) viscoelastic solutions that verifies the potential of PEO to be used in impedance-based viscoelastic flow cytometry. Particles are aligned at the center of the channel at 40 μl/h and maintained their central trajectories at 200 μl/h. At 1900 μl/h, particles are dislocated from their central position due to high influence of inertial lift force similar to 1X PBS experiment.

Based on these results we conclude that the amount of ionic concentration, in the range we tested, has no observable influence on the rheological properties of the viscoelastic solution or the particle focusing performance. Thus, the synthetic polymer PEO is a good candidate for viscoelastic based particle focusing for impedance cytometry applications.

Next, we investigated the viscoelastic focusing behavior for human RBCs that will potentially pave the way to numerous applications for nonspherical particle alignment and impedance based measurements. We suspended the RBCs in 1X-PBS/PEO solution and observed the particle focusing efficiency for increasing flow rates. The suspension was pumped through the channel with a pressure pump (Elveflow OB1). Snapshots from the recorded videos at specific flow rates are given in Fig. 3C, which depicts the trajectory of RBCs along the microchannel. Elastic force is weak at very low flow rates (~0.6 μl/h). When flow rate is increased to 2.6 μl/h, RBCs are partially aligned to a single trace. At 5.5 μl/h (Re: ~0.02), a fully aligned single trace of RBCs is achieved at the centerline of the channel. The focused RBCs form a parachute shape when the flow rate is between ~15 to 30 μl/h (0.07<Re<0.15). At higher flow rates, 40 μl/h (Re: 0.2), we observed deterioration of focusing trajectory. At such flow rates, high elastic force causes excessive stretching on deformable RBCs, which corresponds to a decrease in the hydrodynamic dimeter [21]. Since the lateral particle migration in viscoelastic flow depends on the ratio of particle size to the channel height, viscoelastic focusing is not achieved at such an extreme size reduction.

In summary, PS beads were aligned at the four corners together with the centerline at 10 μl/h (Re: 0.017). Centerline alignment was achieved in the range of 0.17<Re<4.0. However, RBCs are focused only at the centerline in the range of 0.02<Re<0.2. This difference originates from the highly deformable structure of RBCs, which are exposed to both elastic and deformation induced wall lift force. The

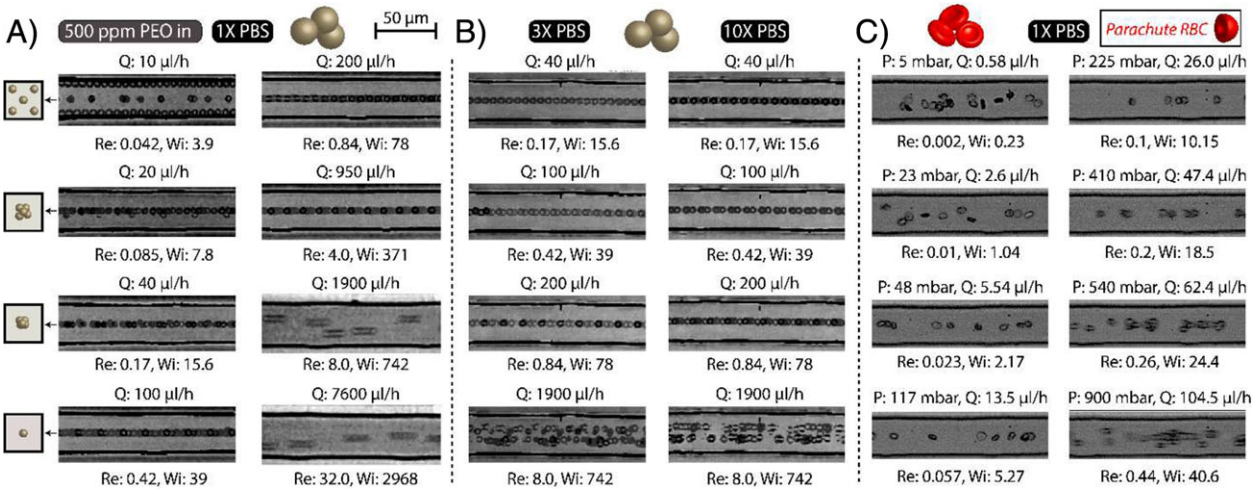

Figure 3. Image stacks of focusing of 6 μm diameter PS beads and RBCs. (A) PS beads suspended in 500 ppm, PEO_{5MDa} dissolved in 1X PBS solution. At low flow rates particles are aligned at the corners and the center of the channel. At higher flow rates up to 950 μl/h elasto-inertial particle focusing is observed. At flow rates above 1900 μl/h, inertial effects dominate and particles are dislocated from the central trajectory. (B) PS beads suspended in 500 ppm, PEO_{5MDa} dissolved in 3X and 10X PBS solutions. A similar profile is achieved as in case a), hence viscoelastic particle focusing efficiency is immune to ionic salt concentration change. (C) RBCs suspended in 500 ppm, PEO_{5MDa} dissolved in 1X PBS solution. Single cell trajectory was obtained at ~50 mbar pressure and 5.5 μl/h flow rate. Parachute shape orientation of RBCs was observed at ~20 μl/h flow rate. For flow rates at 40 μl/h and higher, cell focusing trajectory was dislocated from the center of the channel. The theory and calculations of relaxation time, dimensionless numbers and flow rates are given in supplementary document, sections S.2 and S.3.

wall lift force is induced by the asymmetrical deformation of particles when they are very close to the channel wall. Eventually, deformable particles are pushed away from the corners to the center of the channel [28].

3.4 Impedance based cytometry measurements

The impedance measurements are based on the sensing of differential change on electrical signal when particles pass over the electrodes and interact with the electric field. The particle transition time was defined by the time difference between signal maximum and minimum points. The voltage signal amplitude is related to the size of the particle since the cell membrane behaves as a barrier and electric field does not penetrate into the cell at low frequencies (≤2 MHz). Therefore, peak-to-peak amplitude of the signal is a characteristic of cell size.

Differential impedance measurements have been performed using 6 μm diameter PS beads and human RBCs in 1X-PBS/PEO based viscoelastic solutions. The solutions were introduced to the channel using a pressure pump set at 50 mbar. Fig. 4 gives read-out signals, close-up views for single particle events, and histogram plots of transit time and peak amplitude. For PS beads, 60 events were collected in 1 min of measurement. The close-up of a single event shows the differential measurement waveform. The transit time for the focused beads is accumulated around 10–12 ms; two events occurred at 16 and 22 ms. Unlike time measurements, voltage signal amplitude shows narrower distribution and is accumulated at ~0.02 mV level. Higher amplitude events rarely occurred. Higher transit time variation is the evidence of insufficient particle focusing at the center of the channel. 50 mbar pressure corresponds to 5–6 μl/h flow rate at which particles are under the influence of viscoelastic focusing (corners and center equilibrium positions for suspended rigid particles) far from elasto-inertial regime. The larger variation in the signal amplitude is a clue of particle clusters (doublets, triplet etc.). Obtaining integer multiples of signal levels, such as two (~0.04 mV), three (~0.06 mV), and four (~0.08 mV) folds of the main signal (~0.02 mV), confirms the aggregation of particles. It is well-known that the signal amplitude is a strong function of solution conductivity, which depends on PBS concentration in our case. We performed viscoelastic focusing and impedimetric detection of PS beads in 3X and 10X PBS/PEO solutions as well and expectedly obtained higher signal to noise ratio with increasing PBS concentration as explained in the Supporting Information document, Section S.4.

Measurements at higher flow rates were performed to understand the behaviour of viscoelastic focusing and the corresponding signal change. The inlet pressure was varied as 50, 100, 150, 200 mbar for PS beads; and 50, 100, 150, 200, 250, 300, 410 mbar for RBCs. The statistical comparison of transit time and signal amplitude for all pressure levels are summarized as mean value, standard deviation, and %CV in Fig. 5A and B. To isolate particle clumps, a gated window was selected for %CV calculations, which removes the statistical outliers while including more than 90% of the events. The mean values of transit time for both PS beads and RBCs decrease with increasing pressure. Corresponding

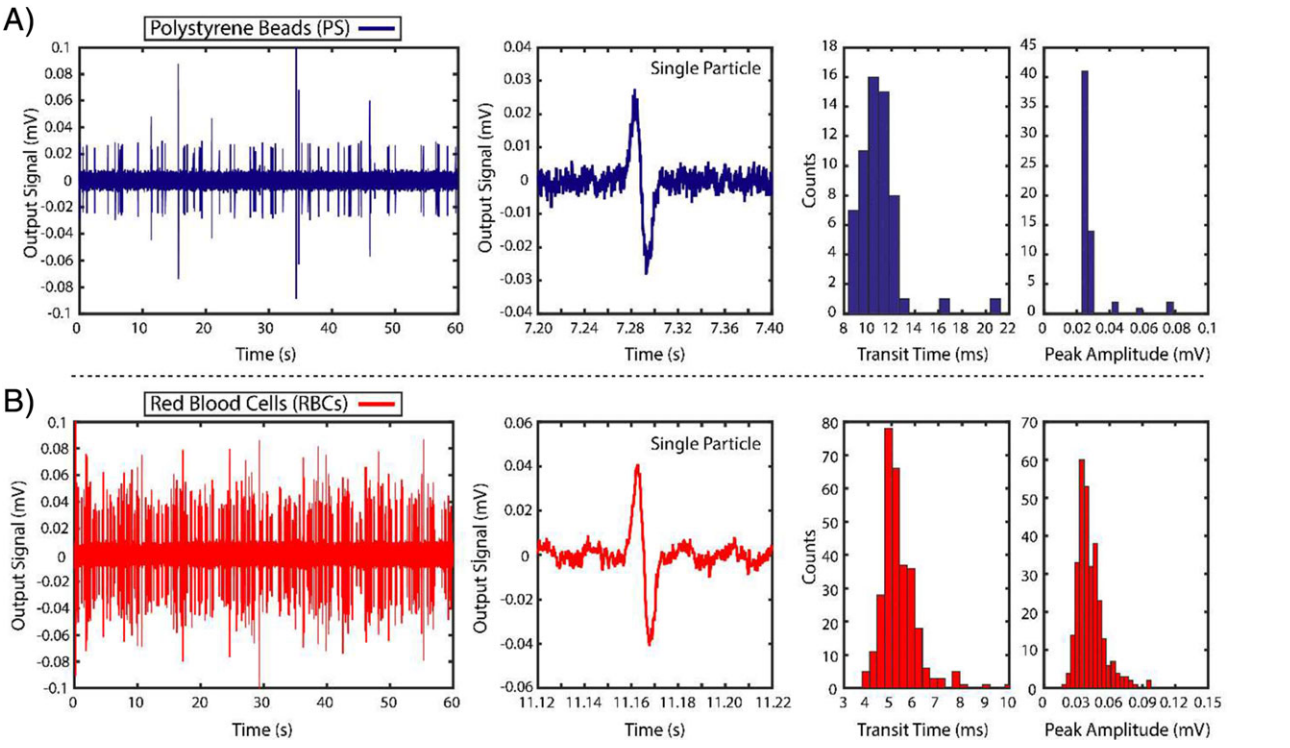

Figure 4. (Left) Impedance cytometry results for (A) PS beads and (B) RBCs at 50 mbar inlet pressure. (Middle) Close-up images of single particle events showing the characteristic differential impedance signal profile. (Right) Histogram plots of transit time and peak amplitudes corresponding to all events.

CV values are approximately 10–15% for both particles. The signal amplitude for PS beads is similar for increasing flow rates showing that viscoelastic focusing is stably maintained. However, %CV for the peak amplitude of RBCs shows greater change at the two points: ~20% increase from 100 to 150 mbar and ~30% increase from 250 to 300 mbar. We have previously shown in Fig. 3C that RBCs start to deform into a parachute shape above ~100 mbar. When the inlet pressure reaches to 250 mbar, all the RBCs get to the same shape. The results given in Fig. 5B show that aligning RBCs into a single orientation leads to more position sensitive and precise measurements. Moreover, when the pressure is above 400 mbar, flow focusing is disturbed due to excessive size stretching of cells and corresponding hydraulic diameter reduction. This behaviour leads to discontinuity of single train of viscoelastic focusing and gives higher measurement variation and %CV values.

In Fig. 5C, transit time versus peak amplitude scatter plots are given for RBCs at selected pressure rates. The throughput is 600, 1800, 3600, and 5700 RBCs/min for 100, 150, 250, and 410 mbar, respectively. At all pressure rates except 410 mbar, peak amplitudes are populated at ~0.04 ± 0.01 mV; there is a side population at ~0.06 mV with the same transition time range. At 410 mbar, ~0.06 mV peak amplitude reaches to the highest number of population. These results are in line with our previous observations that beyond 410 mbar RBCs are unable to cope with elastic force and lose their trajectory at the center of the channel.

4 Concluding remarks

Herein, we have assessed the effect of ionic buffer concentration in viscoelastic focusing using both rheometer measurements and focusing trajectories in square cross-sectional microfluidic channels at varying flow rates. Ionic concentration rate is critical for cell viability and impedance measurements. We concluded that shear viscosities and focused particle trajectories showed no observable dependency to the concentration of PBS from 1X to 10X. These results verify that PEO viscoelastic solutions are good candidates for impedance based measurement applications as opposed to polyelectrolyte viscoelastic solutions, such as HA, which have high rheological dependency on ionic concentration of the solution (data shown in Supporting Information document).

We optimized the PEO_{5MDa} viscoelastic solution at 500 ppm concentration for efficient particle focusing. Elasto-inertial particle focusing at high Reynolds number (Re: 4.0) was successfully achieved for PS beads. The focusing of RBCs was possible at considerably low Reynolds number (Re<0.2). Additionally, parachute shape single RBC orientation is achieved at Re: 0.1. Achieving fixed particle orientation for nonspherical objects is very critical in cytometry applications to get low signal variations. By tuning the properties of the viscoelastic solution, we were able to achieve this property for a range of flow rates.

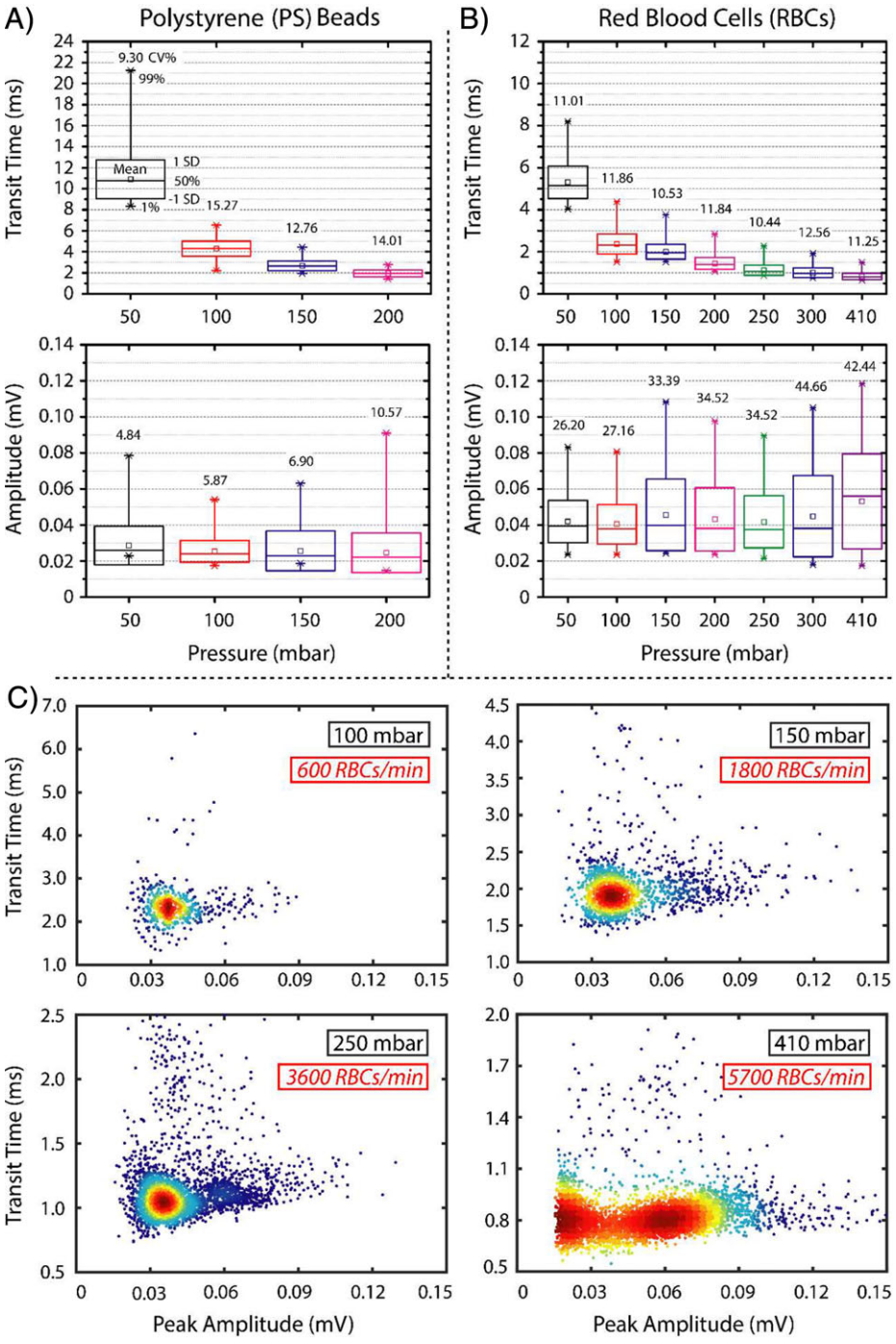

Figure 5. Bar chart representation of transit time, peak amplitude, and %CV of (A) PS beads and (B) RBCs detected at varying inlet pressures. For each bar graph, the *square* represents the mean value, the *box* represents the standard deviation, and the *whisker lines* represent the 99% and 1% population of the counted events. (C) Scatter plots of transit times vs peak amplitudes at four inlet pressures for RBC impedance measurements. Comparison of the transit time, impedance peak amplitude, and % CV at different inlet pressures for both particle types are tabulated in Supporting Information document, Section S.5.

Finally, we performed impedance cytometry measurements for PS beads and RBCs. For the first time in the literature, we married the viscoelastic particle focusing technique with an impedance based microfluidic cytometry device. We achieved 3600 cells/min throughput for RBC characterization.

Viscoelastic focusing addresses the need for single train of particle trajectory required for planar electrode configuration impedance based cytometry systems. Obtaining a single stable orientation for nonspherical particles differentiates viscoelastic focusing from other focusing techniques. The simplicity of viscoelastic focusing with the combination of impedance measurement results in a powerful tool for cell counting and sizing applications. This method is specifically useful for morphology-based characterization of disease-infected cells.

The authors thank to Zeynep Erdogan, Ziya Isiksacan for contributions during rheometer measurements and preparation

of the manuscript. The authors acknowledge support from Kutay Icoz, Urartu S. Seker, Recep Ahan and Elif D. Ergul for biological experiments. The detection system was acquired by financial support from the Scientific and Technological Research Council of Turkey (TÜBITAK, Project No. 215E086).

The authors have declared no conflict of interest.

5 References

[1] Holmes, D., Morgan, H., Green, N. G., *Biosens. Bioelectron.* 2006, *21*, 1621–1630.

[2] Yan, S., Zhang, J., Li, M., Alici, G., Du, H., Sluyter, R., Li, W., *Sci. Rep.* 2014, *4*, 5060.

[3] Shi, J., Mao, X., Ahmed, D., Colletti, A., Huang, T. J., *Lab Chip* 2008, *8*, 221–223.

[4] Shi, J., Yazdi, S., Lin, S.-C. S., Ding, X., Chiang, I.-K., Sharp, K., Huang, T. J., *Lab Chip* 2011, *11*, 2319–2324.

[5] Liang, L., Xuan, X., *Microfluid. Nanofluidics* 2012, *13*, 637–643.

[6] Lin, Y. H., Lee, G. Bin, *Biosens. Bioelectron.* 2008, *24*, 572–578.

[7] Tang, W., Tang, D., Ni, Z., Xiang, N., Yi, H., *Anal. Chem.* 2017, *89*, 3154–3161.

[8] Hur, S. C., Tse, H. T. K., Di Carlo, D., *Lab Chip* 2010, *10*, 274–280.

[9] Yang, S., Kim, J. Y., Lee, S. J., Lee, S. S., Kim, J. M., *Lab Chip* 2011, *11*, 266–273.

[10] D'Avino, G., Romeo, G., Villone, M. M., Greco, F., Netti, P. A., Maffettone, P. L., *Lab Chip* 2012, *12*, 1638–1645.

[11] Seo, K. W., Byeon, H. J., Huh, H. K., Lee, S. J., *RSC Adv.* 2014, *4*, 3512–3520.

[12] Nam, J., Namgung, B., Lim, C. T., Bae, J. E., Leo, H. L., Cho, K. S., Kim, S., *J. Chromatogr. A* 2015, *1406*, 244–250.

[13] Abdulla, A., Liu, W., Gholamipour-Shirazi, A., Sun, J., Ding, X., *Anal. Chem.* 2018, *90*, 4397–4405.

[14] Wang, X., Gao, H., Dindic, N., Kaval, N., Papautsky, I., *Biomicrofluidics* 2017, *11*, 014107.

[15] Bhagat, A. A. S., Kuntaegowdanahalli, S. S., Kaval, N., Seliskar, C. J., Papautsky, I., *Biomed. Microdevices* 2010, *12*, 187–195.

[16] Kim, J., Lee, J., Wu, C., Nam, S., Di Carlo, D., Lee, W., *Lab Chip* 2016, *16*, 992–1001.

[17] Paiè, P., Bragheri, F., Di Carlo, D., Osellame, R., *Microsystems Nanoeng.* 2017, *3*, 17027.

[18] Holzner, G., Stavrakis, S., DeMello, A., *Anal. Chem.* 2017, *89*, 11653–11663.

[19] Lu, X., Liu, C., Hu, G., Xuan, X., *J. Colloid Interface Sci.* 2017, *500*, 182–201.

[20] Yuan, D., Zhao, Q., Yan, S., Tang, S.-Y., Alici, G., Zhang, J., Li, W., *Lab Chip* 2018, *18*, 551–567.

[21] Lim, E. J., Ober, T. J., Edd, J. F., Desai, S. P., Neal, D., Bong, K. W., Doyle, P. S., McKinley, G. H., Toner, M., *Nat. Commun.* 2014, *5*, 4120.

[22] Ahn, S. W., Lee, S. S., Lee, S. J., Kim, J. M., *Chem. Eng. Sci.* 2015, *126*, 237–243.

[23] Kim, B., Kim, J. M., *Biomicrofluidics* 2016, *10*, 024111.

[24] Lu, X., Xuan, X., *Anal. Chem.* 2015, *87*, 6389–6396.

[25] Xiang, N., Zhonghua, N., Hong, Y., *Electrophoresis* 2018, *39*, 417–424.

[26] Seo, K. W., Ha, Y. R., Lee, S. J., *Appl. Phys. Lett.* 2014, *104*, 213702.

[27] Nam, J., Lim, H., Kim, D., Jung, H., Shin, S., *Lab Chip* 2012, *12*, 1347–1354.

[28] Yang, S., Lee, S. S., Ahn, S. W., Kang, K., Shim, W., Lee, G., Hyun, K., Kim, J. M., *Soft Matter* 2012, *8*, 5011–5019.

[29] Liu, C., Ding, B., Xue, C., Tian, Y., Hu, G., Sun, J., *Anal. Chem.* 2016, *88*, 12547−12553.

[30] Go, T., Byeon, H., Lee, S. J., *Sci. Rep.* 2017, *7*, 41162.

[31] Liu, C., Xue, C., Hu, G., *Procedia Eng.* 2015, *126*, 721–724.

[32] Tung, C. K., Lin, C., Harvey, B., Fiore, A. G., Ardon, F., Wu, M., Suarez, S. S., *Sci. Rep.* 2017, *7*, 3152.

[33] Del Giudice, F., Sathish, S., D'Avino, G., Shen, A. Q., *Anal. Chem.* 2017, *89*, 13146–13159.

[34] Faridi, M. A., Ramachandraiah, H., Banerjee, I., Ardabili, S., Zelenin, S., Russom, A., *J. Nanobiotechnol.* 2017, *15*, 1–9.

[35] Kim, J. S., Anderson, G. P., Erickson, J. S., Golden, J. P., Nasir, M., Ligler, F. S., *Anal. Chem.* 2009, *81*, 5426–5432.

[36] Li, D., Lu, X., Xuan, X., *Anal. Chem.* 2016, *88*, 12303–12309.

[37] Kang, K., Lee, S. S., Hyun, K., Lee, S. J., Kim, J. M., *Nat. Commun.* 2013, *4*, 2567–2568.

[38] Sun, T., Morgan, H., *Microfluid. Nanofluid.* 2010, *8*, 423–443.

[39] Guler, M. T., Bilican, I., *Sens. Actuators A* 2018, *269*, 454–463.

[40] Guler, M. T., Bilican, I., Agan, S., Elbuken, C., *J. Micromech. Microeng.* 2015, *25*, 095019.

[41] Etcheverry, S., Faridi, A., Ramachandraiah, H., Kumar, T., Margulis, W., Laurell, F., Russom, A., *Sci. Rep.* 2017, *7*, 5628.

[42] Asghari, M., Serhatlioglu, M., Ortaç, B., Solmaz, M. E., Elbuken, C., *Sci. Rep.* 2017, *7*, 12342.

[43] Li, D., Xuan, X., *Microfluid. Nanofluid.* 2018, *22*, 22–49.

[44] Yu, D. M., Amidon, G. L., Weiner, N. D., Goldberg, A. H., *J. Pharm. Sci.* 1994, *83*, 1443–1449.

